Magnetism and structure of Li_xCoO_2 and comparison to Na_xCoO_2

J. T. Hertz,[1] Q. Huang,[2] T. McQueen,[1] T. Klimczuk,[3,4] J. W. G. Bos,[5] L. Viciu,[1] and R. J. Cava[1]
[1]*Department of Chemistry, Princeton University, Princeton, New Jersey 08544, USA*
[2]*Center for Neutron Research, NIST, Gaithersburg, Maryland 20899, USA*
[3]*Division of Thermal Physics, Los Alamos National Laboratory, Los Alamos, New Mexico 87545, USA*
[4]*Faculty of Applied Physics and Mathematics, Gdansk University of Technology, Narutowicza 11/12, 80-952 Gdansk, Poland*
[5]*School of Chemistry and Centre for Science at Extreme Conditions, University of Edinburgh, Edinburgh EH9 3JJ, United Kingdom*
(Received 19 October 2007; revised manuscript received 19 January 2008; published 19 February 2008)

The magnetic properties and structure of Li_xCoO_2 for $0.5<x<1.0$ are reported. Co^{4+} is found to be high spin in Li_xCoO_2 for $0.94\leqslant x\leqslant 1.00$ and low spin for $0.50\leqslant x\leqslant 0.78$. Weak antiferromagnetic coupling is observed, and at $x\approx 0.65$ the temperature-independent contribution to the magnetic susceptibility and the electronic contribution to the specific heat are largest. Neutron diffraction analysis reveals that the lithium oxide layer expands perpendicular to the basal plane and the Li ions displace from their ideal octahedral sites with decreasing x. Comparison of the structures of Na_xCoO_2 and Li_xCoO_2 reveals that the CoO_2 layer changes substantially with alkali content in the former but is relatively rigid in the latter, and that the CoO_6 octahedra in Li_xCoO_2 are less distorted.

DOI: 10.1103/PhysRevB.77.075119 PACS number(s): 75.47.Pq, 75.20.Hr, 61.05.fm, 61.66.Fn

INTRODUCTION

Na_xCoO_2 has recently been under intense study because it exhibits anomalously high thermopower,[1] superconductivity when intercalated with water,[2] and an unexpected metal-insulator transition,[3] motivating investigation into the relationships between its structure and properties (see, e.g., Refs. 4–9). As the sodium content is varied, the coordination of the sodium ions, the CoO_2 layer alignment, and the unit cell parameters change considerably, and have been correlated to trends in the electronic and magnetic behavior via structural distortions of the CoO_2 layer.[4,10] Li_xCoO_2 system has been studied extensively in rechargeable battery applications (see, e.g., Refs. 11–13), but significantly less attention has been paid to its structural, electronic, and magnetic properties.

Three forms of $LiCoO_2$ have been reported.[14–18] The present investigation is limited to the thermodynamically stable three-layer HT-$LiCoO_2$ phase, which is structurally analogous to three-layer $NaCoO_2$. When lithium ions are removed from $LiCoO_2$ to form Li_xCoO_2,[19–29] $1-x$ cobalt atoms are formally oxidized to Co^{4+}. HT-$LiCoO_2$ has the layered α-$NaFeO_2$-type structure, space group R-3m, consisting of sheets of Co^{3+}-based edge-sharing CoO_6 octahedra separated from one another by sheets of Li^+. The Li^+ occupy octahedral sites between the oxygen of adjacent cobalt oxide layers. The CoO_2 layers stack in an *ABCABC* fashion, and one unit cell of $LiCoO_2$ contains three layers.[30–32] Some magnetic characterization of Li_xCoO_2 has previously been reported,[21,33–37] as an insulator to metal transition[29] that has been examined by density functional theory,[38] but comprehensive structure-property correlations have not yet been established. The spin state of Co^{3+} and Co^{4+} ions in oxides is a matter of active study, but such ions are generally found to be in their low-spin d^6 and d^5 configurations in compounds such as Li_xCoO_2 and Na_xCoO_2.[1,39–44]

The present study characterizes Li_xCoO_2 in the range $0.5\leqslant x\leqslant 1.0$, the compositions accessible to soft chemistry methods.[25,45] Previous studies have shown that Li_xCoO_2 maintains a three-layered structure for $0.54\leqslant x\leqslant 1.00$, with a mixture of two phases in the range $0.78\leqslant x\leqslant 0.94$.[25–27,46] A monoclinic distortion has been observed in the region $0.46<x<0.54$.[26–28] The structure of this monoclinically distorted compound has been studied by electron diffraction,[28] and the structures of some other members of the Li_xCoO_2 system have been studied by x-ray diffraction.[32] Here, we present the magnetic and structural characterizations of a uniform series of Li_xCoO_2 samples, comparing those results to the same characteristics in Na_xCoO_2, with the aim of establishing broad structure-property correlations in electronic systems based on hexagonal CoO_2 planes.

EXPERIMENT

The $LiCoO_2$ used in the present study was synthesized by previously established methods (e.g., Refs. 19–21, 47, and 48). Stoichiometric amounts of Li_2CO_3 (Alfa Aesar, 99%) and Co_3O_4 (Alfa Aesar, 99.7%) were combined and mixed thoroughly. The mixture was placed in a covered alumina crucible, heated to 900 °C, and held for 24 h under a slow flow of oxygen. The samples were then furnace cooled, thoroughly ground, and heated at 900 °C for another 24 h under flowing oxygen. The purity of the $LiCoO_2$ was confirmed by powder x-ray diffraction (Bruker D8 focus, Cu $K\alpha$ radiation, diffracted beam graphite monochromator). Powder x-ray diffraction patterns were also used to characterize the crystallographic cell parameters of the deintercalated samples. Internal silicon standards were employed, and unit cell refinement was accomplished using TOPAS (Bruker XRD) software.

In some previously reported syntheses of $LiCoO_2$, a small excess of lithium carbonate was used to counterbalance loss of lithium oxide, which vaporizes at high temperatures.[19,21,23] The use of excess Li_2CO_3 is important in the present study, because Li excess $Li_{1+x}CoO_2$ has been previously reported.[37] In agreement with that study, we find that the magnetic properties near $x=1$ in Li_xCoO_2 are dependent on the initial mixture of starting materials. In order to evaluate the effects of

using excess lithium on the synthesis and magnetic properties of $LiCoO_2$, six samples of $LiCoO_2$ were prepared as described above using 0%, 4%, 5%, 8%, 10%, and 12% molar excess Li_2CO_3.

For the magnetic susceptibility and specific heat studies, a 10 g master batch of nominally stoichiometric $LiCoO_2$ was synthesized. For the deintercalation of the starting material, 0.5 g samples of $LiCoO_2$ were reacted with different amounts of liquid Br_2 (Alfa Aesar, 99.8%). Between 0.05 and 2.5 ml of bromine was added to each 0.5 g sample of $LiCoO_2$ in 10 ml of acetonitrile, and the reaction mixture was stirred for three days.[49] The deintercalated samples were filtered, washed with acetonitrile, and dried under aspiration. All Li_xCoO_2 samples with compositions between $x=0.5$ and $x=1.0$ were found to be stable in dry air. For determination of the Li content, 4 mg of each Li_xCoO_2 sample was dissolved in 2 ml of HCl and diluted with 18 ml of de-ionized H_2O. ICP-AES analysis was performed using a Perkin Elmer Optima 4300 ICP-AES and powder x-ray diffraction was performed.[50]

For neutron diffraction measurements, a second 10 g master batch of nominally stoichiometric $LiCoO_2$ was synthesized. Five samples of Li_xCoO_2 ($0.5 \leqslant x \leqslant 1.0$) were then made by reacting 2 g aliquots of this $LiCoO_2$ with the Br_2 oxidant solutions. One of the samples used in the neutron diffraction study was selected to be within the two-phase region ($0.78 \leqslant x \leqslant 0.94$),[12,26,51,52] so that the structures of the Li_xCoO_2 compounds at the border compositions ($x=0.78$ and $x=0.94$) could be determined.

Neutron diffraction analysis was performed at the NIST Center for Neutron Research on the BT1 diffractometer. The powder neutron diffraction patterns at 298 K were obtained using a Cu (311) monochromator with a 90° take-off angle, $\lambda=1.5404(2)$ Å, and in-pile and diffracted beam collimations of 15′ and 20′, respectively. Data were collected over the two theta range 3°–168° with a step size of 0.05°. The GSAS program suite was used for Rietveld structural refinement.[53] Scattering lengths (in fm) employed in the refinement were −1.90, 2.49, and 5.80 for Li, Co, and O, respectively.

The magnetic susceptibilities and specific heats of the samples were measured in a Quantum Design Physical Properties Measurement System. Specific heat measurements were performed on six of the Li_xCoO_2 samples used for magnetic analysis ($x=1.00$, 0.78, 0.70, 0.62, 0.58, and 0.51). About 25 mg of sample powder was mixed with an equal mass of Ag powder, and then pressed into a pellet. The use of silver was necessary because Li_xCoO_2 samples are poor thermal conductors. The specific heat of each sample was measured at low temperatures ($2\ \mathrm{K} \leqslant T \leqslant 15\ \mathrm{K}$), and the contribution of the Ag powder was subtracted.

MAGNETISM AND STOICHIOMETRY IN $LiCoO_2$

The laboratory powder x-ray diffraction patterns obtained from the samples of $LiCoO_2$ synthesized with excess Li_2CO_3 were virtually indistinguishable from the pattern obtained from the sample synthesized with no excess lithium, indicating that the samples possess very similar structures and lattice parameters. Thus, the crystal structure of the product

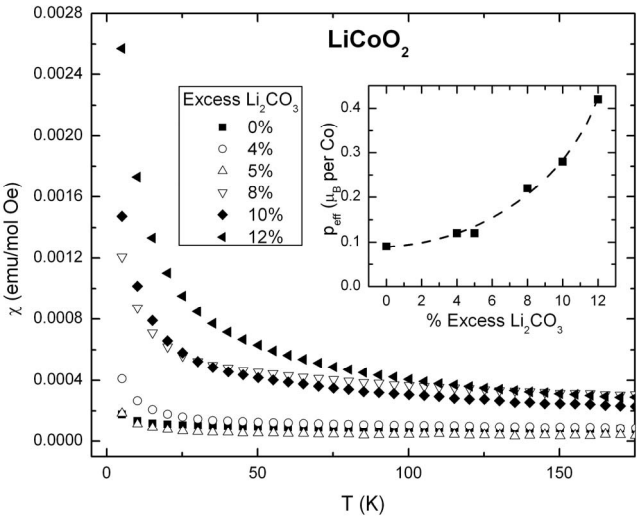

FIG. 1. Temperature-dependent magnetic susceptibility of $LiCoO_2$ for samples made with various amounts of excess Li_2CO_3. Inset: The effective magnetic moments per Co of the nominal $LiCoO_2$ samples plotted vs the amount of excess Li_2CO_3 used in the synthesis.

was not strongly affected by the amount of excess lithium present in the reaction mixture. Furthermore, none of the x-ray diffraction (XRD) patterns contained detectable impurity peaks, indicating that a lithium-rich impurity phase did not form in significant proportion in any of the samples. Laboratory XRD analysis, therefore, provided little information about how much, if any, excess Li_2CO_3 is needed to synthesize stoichiometric $LiCoO_2$. Magnetic measurements, which are more sensitive, were therefore used to distinguish the samples.

The average oxidation state of cobalt is directly related to the amount of lithium in the compound. If lithium is lost to vaporization during synthesis and Li_xCoO_2 ($x<1.00$) is formed, then $1-x$ cobalt atoms will be oxidized to Co^{4+}. Similarly, if extra lithium is incorporated into a compound of either $Li_{1+x}CoO_2$ or $Li_{1+x}Co_{1-x}O_2$ ($x>0$), then x ($2x$) cobalt atoms will be reduced (oxidized) to Co^{2+} (Co^{4+}) to maintain charge neutrality. Thus, if a nonstoichiometric amount of Li is incorporated into $LiCoO_2$, the sample will show a magnetic moment: Only perfectly stoichiometric $LiCoO_2$ will show no local moment because its Co^{3+} is in a low-spin d^6 configuration. By measuring the magnetic susceptibilities of the six samples made with varying amounts of Li_2CO_3, it was possible to determine which sample was least magnetic and thus closest to stoichiometric $LiCoO_2$.

The results of the magnetic susceptibility measurements on these samples are displayed in Fig. 1. As the figure shows, the samples become more magnetic with increasing Li_2CO_3. Curie-Weiss fits were performed using $\chi=\chi_0+C/(T-\theta_{CW})$, where χ and χ_0 are the measured and temperature-independent parts of the susceptibility, C is the Curie constant, T is temperature in Kelvin, and θ_{CW} is the Curie-Weiss temperature. The calculated effective magnetic moments per Co for each of the six samples are displayed in the inset of Fig. 1. The use of excess Li_2CO_3 results in the presence of a

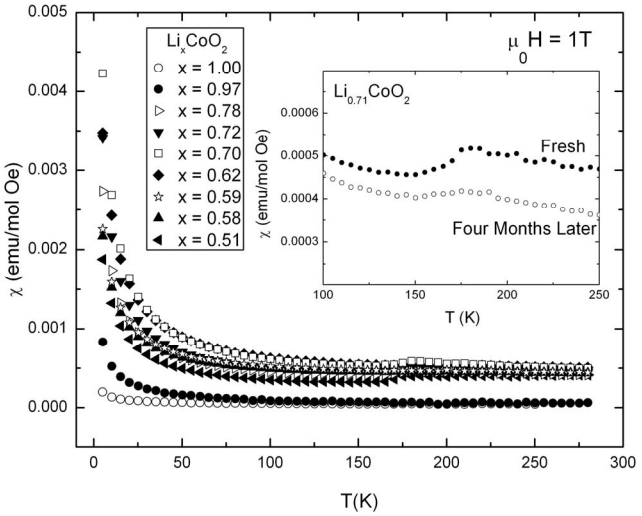

FIG. 2. Temperature-dependent magnetic susceptibilities for Li_xCoO_2 Inset: Comparison of the magnetic susceptibility of $Li_{0.72}CoO_2$ as freshly made and after storage for four months.

magnetic moment that increases in magnitude as higher lithium-containing starting material is used. The least magnetic sample was the one made without excess Li_2CO_3, and, therefore, no excess Li_2CO_3 was used in subsequent syntheses of $LiCoO_2$.

The origin of the observed local moment in the Li excess samples is open to speculation. It has been previously proposed that incorporation of extra lithium results in $Li_{1+x}CoO_2$ ($x>0$) and the reduction of x Co^{3+} atoms to Co^{2+}.[12,17–19] This is unlikely for two reasons. First, all the octahedral sites in the lithium layer are filled in stoichiometric $LiCoO_2$, so there is no room for more due to the Li-Li repulsion. Second, the synthesis is performed in a highly oxidizing environment (due to the presence of flowing oxygen and highly electropositive Li^+), and the reduction of Co^{3+} to Co^{2+} is unlikely. Another proposal is that the excess Li goes on the Co site and is accompanied by the formation of charge-compensating oxygen vacancies to maintain the Co^{3+} state. In this case, the magnetism is proposed to be due to a low-spin to high-spin transition on Co^{3+} induced by the disorder.[37] There is no evidence, however, for the presence of oxygen vacancies in this compound. The most likely explanation is that the excess lithium ions substitute for cobalt in the stoichiometric CoO_2 layer, resulting in $Li_{1+x}Co_{1-x}O_2$ ($x>0$), and the introduction of magnetic Co^{4+}. A quantitative determination of the dependence of the magnetic moment on excess Li concentration in carefully synthesized and characterized Li-excess $LiCoO_2$ would be of further interest to resolve the actual microscopic mechanism of moment formation for this phase.

MAGNETIC PROPERTIES OF Li_xCoO_2

The magnetic properties of Li_xCoO_2 were studied for $x=1.00$, 0.97, 0.78, 0.72, 0.70, 0.62, 0.59, and 0.51. The temperature-dependent susceptibility results are displayed in Fig. 2. The data show several general features. No magnetic

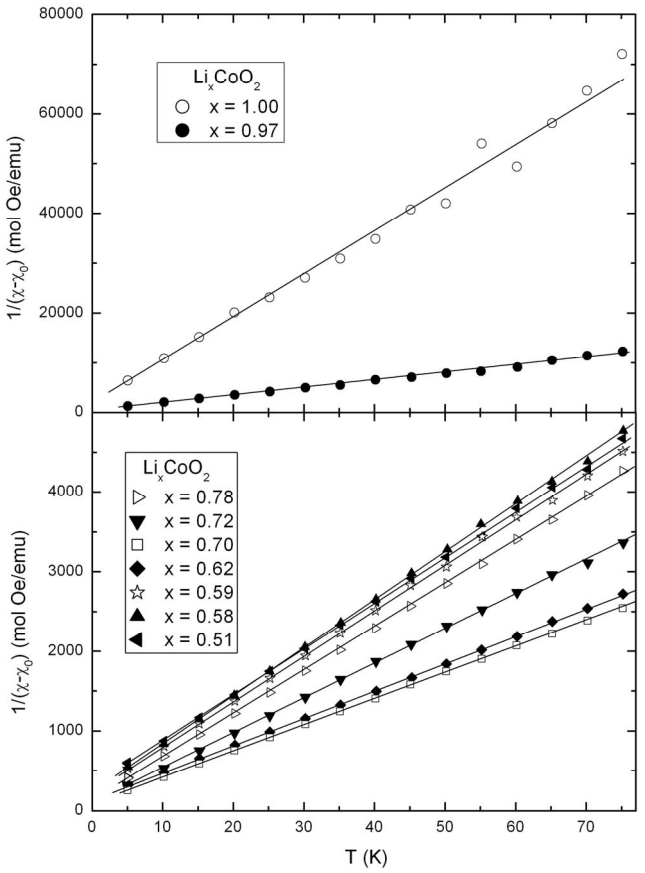

FIG. 3. Upper panel: The temperature dependence of $1/(\chi-\chi_0)$ for the two Li_xCoO_2 samples above the two-phase region over the range 5 K$\leqslant T\leqslant$75 K. Lower panel: The temperature dependence of $1/(\chi-\chi_0)$ for the seven Li_xCoO_2 samples below the two-phase region over the range 5 K$\leqslant T\leqslant$75 K.

ordering is observed in any of the samples down to the lowest temperature measured ($T=5$ K). All Li_xCoO_2 samples exhibit Curie-Weiss behavior, and some samples show anomalies at 175 K. The temperature-independent magnetic contribution to the susceptibility increases considerably as the Li content in Li_xCoO_2 decreases to compositions below the two-phase region ($0.5\leqslant x\leqslant 0.78$).

Several previous studies have reported the presence of a susceptibility anomaly at 175 K in Li_xCoO_2 compounds.[33–36] Because this anomaly has been observed in samples with widely ranging Li contents, from $x=0.95$ (Ref. 33) to $x=0.50$, and because the temperature of the anomaly is independent of the Li concentration over that broad range of composition, we investigated whether it might be due to a magnetic impurity. The compounds CoO, Co_3O_4, and $Li_{0.1}Co_{0.9}O$ were tested, as a mixed-phase sample at composition Li_2CoO_x, and none showed a 175 K anomaly. In addition, we remeasured the magnetic susceptibility after four months storage of three of the samples in our study ($x=0.78$, 0.72, and 0.51) that showed the magnetic anomaly. The data for one of the samples are shown in the inset to Fig. 2. Though the crystallographic cell parameters of the samples and overall behavior of the susceptibility were unchanged, indicating that the compounds had not decomposed

TABLE I. Magnetic and electronic characterization of Li_xCoO_2.

Li Content (x)	χ_{280} (emu/mol$_{Co}$ Oe)	Low temp. χ_0 (emu/mol$_{Co}$ Oe)	θ_W (K)	p_{eff} (μ_B/Co)	p_{eff} (μ_B/Co^{4+})	Γ mJ/mol K^{-2}
1.00 (0.985)	0.44×10^{-4}	0.43×10^{-4}	−1.0	0.09	(5.9)	0.4
0.97 (0.961)	0.63×10^{-4}	0.33×10^{-4}	−2.2	0.23	7.67 (5.9)	
0.78	4.14×10^{-4}	2.78×10^{-4}	−2.3	0.38	1.72	12.4
0.72	4.51×10^{-4}	2.71×10^{-4}	−2.3	0.43	1.54	
0.70	4.96×10^{-4}	3.13×10^{-4}	−2.8	0.49	1.63	18.9
0.62	5.08×10^{-4}	3.52×10^{-4}	−4.0	0.48	1.26	19.9
0.59	4.41×10^{-4}	3.52×10^{-4}	−4.1	0.37	0.90	
0.58	4.37×10^{-4}	3.28×10^{-4}	−4.0	0.36	0.86	18.4
0.51	4.11×10^{-4}	1.80×10^{-4}	−5.2	0.37	0.76	14.6

or changed overall compositions substantially, the anomaly was strongly suppressed in all cases. This suggests that the anomaly may be due either to the presence of a small amount of an impurity phase that decomposes slowly in air or that it is intrinsic but sensitive to a subtle change in the structure of the compound over time, as would happen, for example, if the ordering of the Li array was changing or if the samples were becoming more chemically homogeneous with time due to the Li diffusion between particles. Further work to determine the origin of this anomaly would be of interest.

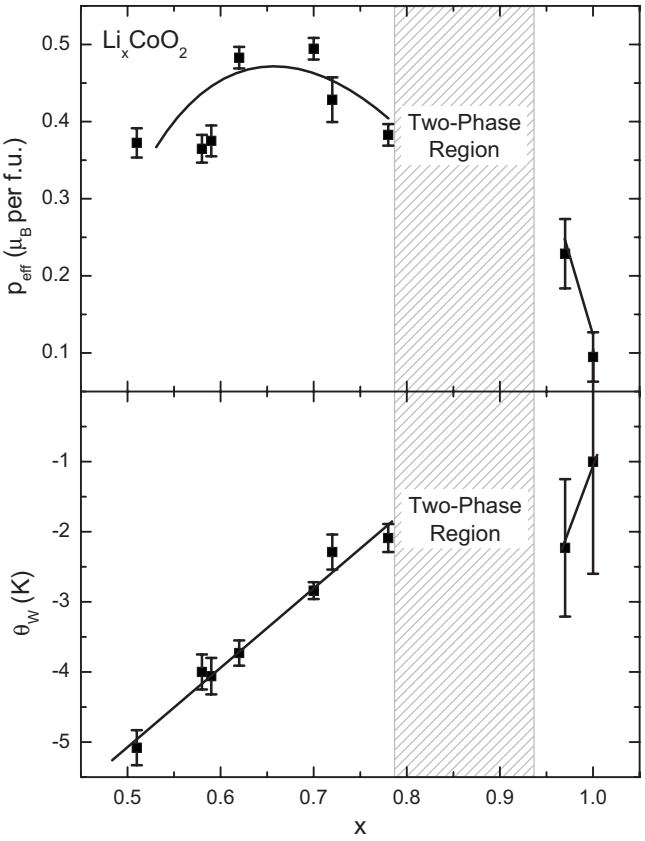

FIG. 4. Upper panel: The variation of p_{eff} per formula unit with x for Li_xCoO_2. Lower panel: The variation of the Weiss temperature (θ_W) with x for Li_xCoO_2.

Figure 2 shows that there is significant local moment character displayed in the susceptibilities of Li_xCoO_2 at low temperatures. The relationship between lithium content and the effective magnetic moment (p_{eff}) was determined by performing Curie-Weiss fits on the low temperature data ($T \leqslant 75$ K). The fitted χ_0 values were used to plot the temperature dependence of $1/(\chi-\chi_0)$ for each of the samples. The results are shown in Fig. 3 for the samples above and below the two-phase region. As expected for Curie-Weiss behavior, the plots are linear. The magnetic characteristics obtained from the fits are presented in Table I.

Figure 4 shows the variation of the effective magnetic moment per formula unit (p_{eff}) with lithium content: p_{eff} increases considerably as lithium is removed until a critical composition is reached ($x \approx 0.65$), then decreases upon further lithium extraction. As Table I and Fig. 4 show, θ_W is small and negative for all of the Li_xCoO_2 samples, suggesting that the Li_xCoO_2 family in the range $0.5 \leqslant x \leqslant 1.0$ is characterized by weak antiferromagnetic interactions that become somewhat stronger as more lithium is extracted.

The extraction of a lithium ion is accompanied by the formal oxidization of a cobalt atom from the nonmagnetic +3 state to the magnetic +4 state, and so, if the unpaired spins remain completely localized, p_{eff} is expected to increase continuously with decreasing lithium content in Li_xCoO_2. The fact that p_{eff} *decreases* as x decreases below 0.65 indicates that there is a changing ratio of local and nonlocal spins in Li_xCoO_2 as a function of composition. This is demonstrated in Fig. 5, which plots the effective magnetic moment per Co^{4+} ion for Li_xCoO_2. If the unpaired spins are localized at all x, then the effective magnetic moment per Co^{4+} should stay constant across the series. As Fig. 5 shows, the effective magnetic moment per Co^{4+} in the composition range $0.7 \leqslant x \leqslant 0.8$ is close to the expected low-spin Co^{4+} spin $\frac{1}{2}$ value of $1.73\mu_B$ (Ref. 54) and remains relatively constant as x first decreases below 0.8. When x drops below 0.65, however, the effective moment per Co^{4+} decreases significantly. We attribute this drop in effective moment to a change in the localization of the unpaired spins at this composition.

As Table I shows, the nominally $Li_{0.97}CoO_2$ sample exhibits an effective magnetic moment of $0.23\mu_B$ per cobalt atom. For $x=0.97$, with 3% of the cobalt atoms in the magnetic +4 oxidation state, this corresponds to a magnetic mo-

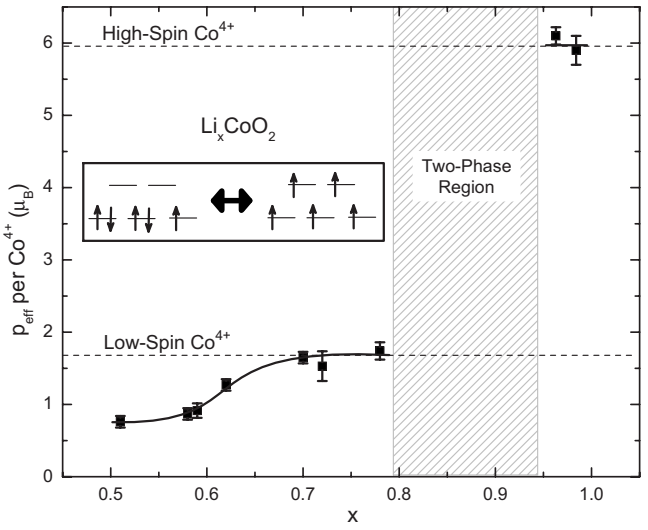

FIG. 5. The variation of the effective magnetic moment per Co^{4+} ion with x for Li_xCoO_2. A high-spin to low-spin transition is observed. Insert: Schematic representation of the change in spin configuration.

ment of $7.67\mu_B$ per Co^{4+}—a value much too large for a low-spin (spin $\frac{1}{2}$) d^5 species. High-spin Co^{4+} has five unpaired electrons and is expected to exhibit an effective magnetic moment of $5.92\mu_B$ (Ref. 54): Our observed effective moment per Co^{4+} for $Li_{0.97}CoO_2$ is even larger. This difference is due to the precision to which the composition is known in the $Li_{0.97}CoO_2$ sample. If the sample instead has a composition of $x=0.961$, within the error range of the determined composition of $x=0.97\pm0.01$, then the effective magnetic moment per Co^{4+} would be $5.9\mu_B$. Our results therefore indicate the presence of high-spin Co^{4+} in Li_xCoO_2 for this composition. (In order for a low-spin Li_xCoO_2 species to exhibit an effective magnetic moment of $0.23\mu_B$, the fraction of Co^{4+} needed would correspond to a Li composition of $Li_{0.868}CoO_2$, well outside the error range of the composition for the sample, and in the chemical two-phase region, which is not the case.) Thus, the nominally $Li_{0.97}CoO_2$ sample contains high-spin Co^{4+} and has an actual composition of $Li_{0.96}CoO_2$.

Similarly, the nominally stoichiometric $LiCoO_2$ sample also exhibits a small magnetic moment, suggesting that it is not perfectly stoichiometric and contains a small number of Co^{4+} ions. In order for a low-spin Li_xCoO_2 species to exhibit the observed effective magnetic moment of $0.09\mu_B$, the fraction of Co^{4+} present would correspond to a lithium content of $x=0.948$, a value again well outside the error range of the composition for the sample ($x=1.00\pm0.02$). If the Co^{4+} ions are high spin, however, then the fraction of Co^{4+} is 0.015. This corresponds to a composition of $Li_{0.985}CoO_2$, or $Li_{1.008}Co_{0.992}O_2$ if excess Li is accommodated, both of which are within the error of the observed composition. Thus, our results indicate that the high x compositions in Li_xCoO_2 contain high-spin Co^{+4}. This analysis implies that the magnetic Co^{4+} introduced by using excess Li in the synthesis of $LiCoO_2$, illustrated in Fig. 1, is also high spin.

Analysis of the magnetic data, therefore, indicates that Li_xCoO_2 samples for low x are low spin, while samples at high x are high spin. This high-spin to low-spin transition, which occurs at the chemical phase boundary, is illustrated in Fig. 5. The nature of the spin state of Co in oxides, especially in the Na_xCoO_2 and Li_xCoO_2 systems, has been the subject of some debate. Numerous recent studies have argued that

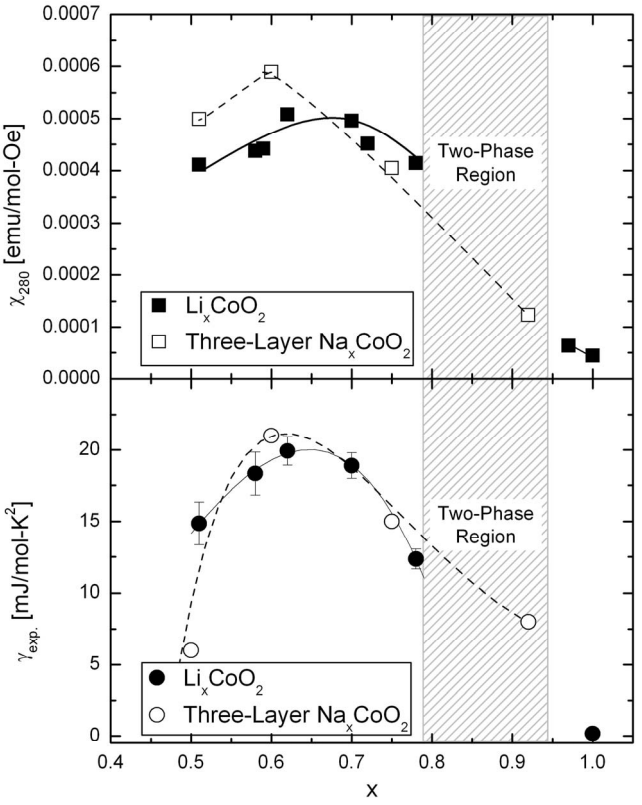

FIG. 6. Upper panel: The variation of the magnetic susceptibility at 280 K (χ_{280}) with x for both Li_xCoO_2 and three-layer Na_xCoO_2 (Ref. 10). Lower panel: The variation of the electronic contribution to the specific heat (γ) with x for both Li_xCoO_2 and three-layer Na_xCoO_2 (Ref. 10). The shaded portion of this figure represents the two-phase region in the Li_xCoO_2 system.

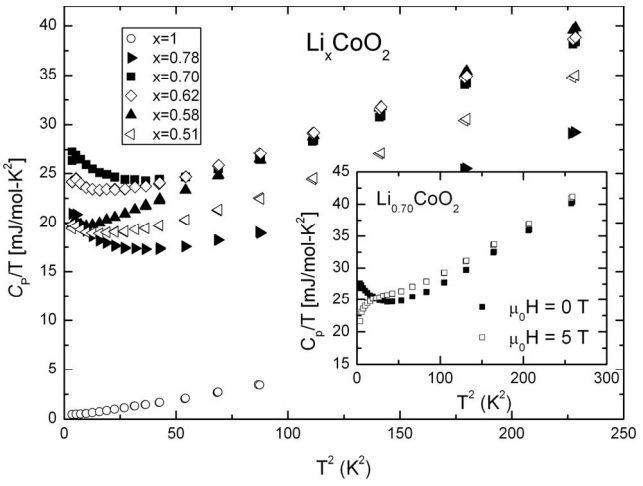

FIG. 7. The specific heat for Li_xCoO_2 plotted as C_P/T versus T^2. Inset: The specific heat for $Li_{0.70}CoO_2$ with $H=0$ T and $H=5$ T.

TABLE II. Refined unit cell parameters for Li_xCoO_2 from the neutron diffraction data.

Compound	Space group	Cell constants (Å)	Unit cell volume (Å^3)	Volume/f.u. (Å^3)
$LiCoO_2$	*R*-3*m* (No. 166)	*a*=2.816 98(3) *c*=14.064 6(1)	96.655(2)	32.22
$Li_{0.94}CoO_2$	*R*-3*m* (No. 166)	*a*=2.815 93(6) *c*=14.060 4(4)	96.554(5)	32.18
$Li_{0.78}CoO_2$	*R*-3*m* (No. 166)	*a*=2.814 96(9) *c*=14.160 9(5)	97.178(6)	32.39
$Li_{0.75}CoO_2$	*R*-3*m* (No. 166)	*a*=2.811 85(3) *c*=14.226 4(4)	97.412(3)	32.47
$Li_{0.66}CoO_2$	*R*-3*m* (No. 166)	*a*=2.811 72(3) *c*=14.286 3(4)	97.812(3)	32.60
$Li_{0.51}CoO_2$	*C*2/*m* (No. 12)	*a*=4.864 5(1) *b*=2.809 64(7) *c*=5.055 1(1) β=107.908(1)°	65.744(4)	32.87

both Co^{3+} and Co^{4+} are low spin in the whole Na_xCoO_2 system[39,55–57] and Li_xCoO_2 system,[35] while some have claimed to observe intermediate-spin[37] or high-spin[34] Co. The case has been argued based on the relative stabilities of electron configurations for Co in octahedral coordination that high-spin Co^{4+} should be stable in these compounds.[58] The fact that Co^{4+} in Li_xCoO_2 above the two-phase region is high spin suggests that these arguments have merit. The structural data, described in a later section, suggest that the spin state transition in Li_xCoO_2 could be driven by a volume effect, since the low-spin Co^{4+} is found in the part of system with shorter Co-O bond lengths, but the differences in bond lengths are subtle and continuous across the transition and so the case for that origin for the spin state transition is weak. The current data appear to present the cleanest case for a high-spin to low-spin transition in the triangular layered CoO_2 family.

We employ the magnetic susceptibility at 280 K (χ_{280}) as a measure of the temperature-independent paramagnetism arising from conduction electrons. The upper panel of Fig. 6 shows the variation of χ_{280} with lithium content. Though χ_{280} does not vary dramatically among the highly delithiated compounds ($0.51 \leqslant x \leqslant 0.78$), it displays a weak peak at a composition $x \approx 0.65$. The temperature-independent susceptibility is an order of magnitude lower for the compounds with Li contents greater than 0.95, indicating that the high x materials have very few free electrons. The upper panel of Fig. 6 also shows the variation of χ_{280} for three-layer Na_xCoO_2.[10] The absolute values of χ_{280} in the range $0.5 \leqslant x \leqslant 1.00$ are quite similar, and the temperature-independent susceptibility increases substantially when more than 10% of the alkali metal is removed from the stoichiometric Co^{3+} compounds for both. The temperature-independent part of the susceptibility is maximized at a similar composition in both systems ($x \approx 0.65$ for Li_xCoO_2, and $x \approx 0.60$ for three-layer Na_xCoO_2), though in Na_xCoO_2 it is more strongly peaked.

Figure 7 displays the low temperature specific heat data for six Li_xCoO_2 samples, plotted as C_P/T vs T^2. The temperature dependence of the specific heat in systems where

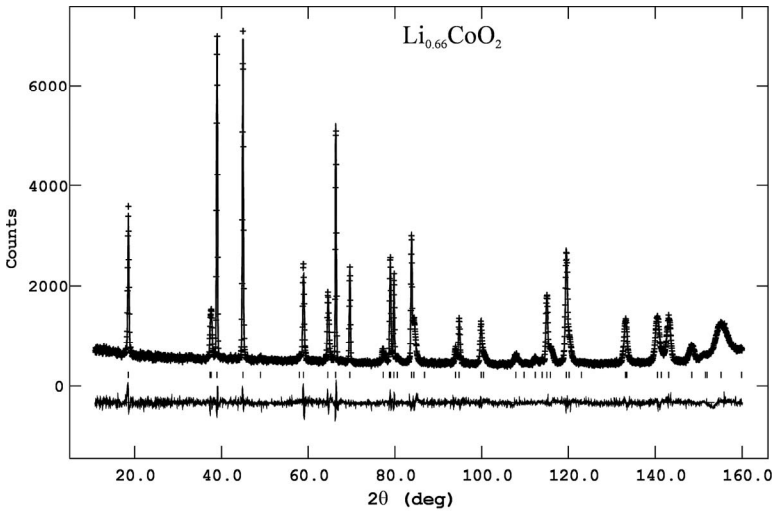

FIG. 8. Observed (points) and calculated (solid line) powder neutron diffraction pattern for $Li_{0.66}CoO_2$ at 298 K. Tic marks indicate the presence of a calculated peak. The lower curve shows the difference between the observed and calculated intensities.

TABLE III. (a) Structural parameters for trigonal Li_xCoO_2 ($x=1$, 0.85, 0.75, and 0.66) at 295 K. Space group: $R\bar{3}m$. Atomic positions: Li: 3*a* (0 0 0), or 18*f* (*x* 0 0), Co: 3*b* (0,0,1/2), and O: 6*c* (0 0 *z*). (b) Structural parameters for monoclinic $Li_{0.51}CoO_2$ at 295 K. Space group: $C2/m$. $a=4.8645(1)$ Å, $b=2.809\,64(7)$ Å, $c=5.0551(1)$ Å, $\beta=107.908(1)°$, $V=64.744(4)$ Å^3.

(a)	Atom	Parameters ($x=$	1.0	0.94, [63.2(2)%][a]	0.78, [36.8(2)%][a]	0.75	0.66
		a (Å)	2.8169 8(3)	2.815 93(6)	2.814 96(9)	2.811 85(3)	2.811 72(3)
		c (Å)	14.064 6(1)	14.060 4(4)	14.160 9(5)	14.226 4(4)	14.286 3(4)
		V (Å^3)	96.655(2)	96.554(5)	97.178(6)	97.412(3)	97.812(3)
	Li	x			0.05(1)	0.066(5)	0.077(4)
		U_{iso} (Å^2)	0.0158(3)	0.013(1)		0.017(2)	0.017(3)
	Co	U_{11}, U_{22} (Å^2)	0.007 4(3)	0.006 2(5)		0.0102(6)	0.0108(5)
		U_{33} (Å^2)	0.007 5(5)	0.014(1)		0.012(1)	0.012(1)
		U_{12} (Å^2)	0.003 7(2)	0.003 1(2)		0.0051(3)	0.0054(3)
	O	z	0.239 49(3)	0.23942(7)	0.2380(1)	0.236 85(6)	0.236 20(6)
		U_{11}, U_{22} (Å^2)	0.008 7(1)	0.008 2(5)		0.011 4(3)	0.011 4(2)
		U_{33} (Å^2)	0.010 2(2)	0.012 4(4)		0.013 5(5)	0.015 6(5)
		U_{12} (Å^2)	0.004 4(1)	0.004 1(4)		0.005 7(1)	0.005 7(1)
		R_p (%)	3.66	3.81		4.76	4.05
		wR_p (%)	4.54	4.73		6.64	5.12
		χ^2	1.054	0.8927		1.769	1.794

(b)	Atom	Site	x	y	z	n	$[U_{iso}]$ U_{11} (Å^2)	U_{22} (Å^2)	U_{33} (Å^2)	U_{13} (Å^2)
	Li	4*h*	0	0.582(3)	$\frac{1}{2}$	0.255	[0.018(3)]			
	Co	2*a*	0	0	0	1	0.006(1)	0.011(1)	0.019(2)	0.004(1)
	O	4*i*	0.7312(2)	0	0.2042(2)	1	0.0093(6)	0.012(5)	0.0197(6)	0.0058(4)
	R_p (%)		3.32							
	wR_p (%)		4.35							
	χ^2		1.842							

[a]Two-phase sample. The temperature factors for Li, Co, and O in two phases were constrained to be equal.

there are electronic and lattice contributions to the specific heat at low temperatures can be written as $C_p/T=\gamma+\beta T^2$, where β and γ are the parameters describing the size of the lattice and electronic contributions to the specific heat, respectively. The values of γ obtained from linear fits to C/T vs T^2 plots are presented in Table I. The data in Fig. 7 are linear at higher temperatures ($T^2>75$ K^2), while at lower temperatures, significant deviations from linearity occur, suggesting that magnetic fluctuations contribute significantly to the specific heat at low temperatures. To further investigate this, specific heat was measured under a 5 T applied field for $x=0.70$ (Fig. 7, inset). Comparison of the 0 and 5 T data suggests that the deviation from linearity is indeed due to the magnetic fluctuations. The lower panel of Fig. 6 depicts the variation of γ with lithium content in Li_xCoO_2 and demonstrates a similarity between the behavior of χ_{280} and γ with composition: γ increases continuously with decreasing lithium content until it is maximized at the previously observed critical composition ($x\approx0.65$). Comparison to the data for Na_xCoO_2 shows similar behavior in the two systems.

CRYSTAL STRUCTURES OF Li_xCoO_2 AND COMPARISON TO Na_xCoO_2

The refinements of the structures of Li_xCoO_2 from the neutron powder diffraction data were straightforward. The compositions of the samples were fixed at the analytically determined chemical compositions. The structure of $LiCoO_2$, with edge-sharing layers of CoO_6 octahedra interleaved with layers of edge-sharing LiO_6 octahedra, provided the initial model for the fits. The refined crystallographic cell parameters from the neutron powder diffraction data are presented in Table II. Structures for Li_xCoO_2 for $x=1.0$, 0.94, 0.78, 0.75, and 0.66 were very well described by the rhombohedral three-layer $LiCoO_2$ structure in space group R-3m (166). A two-phase refinement at overall composition $Li_{0.85}CoO_2$ was employed to determine the structures of the border compositions of the two-phase region, $x=0.94$ and $x=0.78$. The symmetry of $Li_{0.51}CoO_2$ is monoclinic, space group $C2/m$ (12).

The published model for $LiCoO_2$ resulted in an excellent fit to our data for compositions on the high x side of the two-phase region, $x=1.0$ and 0.94. However, refinements for

TABLE IV. Selected bond lengths and bond angles for Li_xCoO_2.

Compound	Co-O bond distance (Å)	O-Co-O bond angle (deg)	Li-O bond distance (Å)	In-plane Co-Co distance (Å)
$LiCoO_2$	1.9220(2)×6	94.24(1)×6 85.75(1)×6	2.0946(3)×6	2.81698(3)
$Li_{0.94}CoO_2$	1.9210(5)×6	94.27(3)×6 85.73(3)×6	2.0944(6)×6	2.81593(6)
$Li_{0.78}CoO_2$	1.9132(8)×6	94.72(5)×6 85.28(5)×6	2.21(2)×2 2.12(2)×2 2.02(2)×2	2.81496(9)
$Li_{0.75}CoO_2$	1.9059(5)×6	95.07(3)×6 84.93(3)×6	2.25(1)×2 2.134(1)×2 2.007(9)×2	2.81185(3)
$Li_{0.66}CoO_2$	1.9032(5)×6	95.24(3)×6 84.76(3)×6	2.284(8)×2 2.147(1)×2 2.000(7)×2	2.81172(3)
$Li_{0.51}CoO_2$	1.8986(9)×2 1.8948(6)×4 Avg: 1.896	95.54(4)×4 95.70(4)×2 84.46(4)×4 84.30(4)×2	2.328(7)×2 2.142(1)×2 2.030(5)×2	2.80909(7)

lower Li content phases showed unacceptably large thermal vibration parameters for the Li atoms, with thermal ellipsoids much larger in the basal plane than perpendicular to the plane. This indicates that the Li are displaced in plane from the centers of their ideal octahedra: the (0,0,0) site for the rhombohedral phases and the $(0,\frac{1}{2},\frac{1}{2})$ site for monoclinic $Li_{0.51}CoO_2$. The refinement of the magnitude of this displacement was significant in all cases and the resulting thermal vibration parameters for the Li assumed normal values. Displacements of the alkali ions from the centers of the coordination polyhedra are commonly seen in Na_xCoO_2 (Ref. 4) and have been seen in a different polymorph of Li_xCoO_2.[15] The agreements between the refined models and the data are excellent (e.g., Fig. 8). The refined atomic positions for lithium, cobalt, and oxygen for all compounds are presented in Tables III(a) and III(b) and selected bond lengths and bond angles are displayed in Table IV.

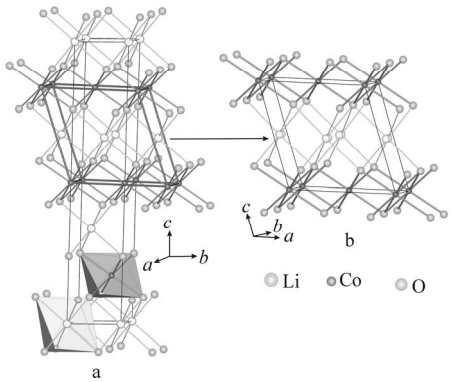

FIG. 9. (a) The rhombohedral crystal structure of $LiCoO_2$. (b) The monoclinic crystal structure of $Li_{0.51}CoO_2$. The partially occupied Li positions, slightly displaced from the centers of the LiO_6 octahedra, are shown. The relationship between the three-layer rhombohedral unit cell and the monoclinic unit cell is also shown.

Monoclinic symmetry crystallographic cells are commonly encountered in layered crystals structures of this type. This occurs when slight shifts of adjacent CoO_2 layers from the ideal positions in a three-layer rhombohedral cell disrupt the threefold symmetry. The Na_xCoO_2 system shows this behavior, for example, Ref. 10. For the Li_xCoO_2 system, this type of monoclinic cell has been previously reported for $0.46 \leqslant x \leqslant 0.54$.[26–28] An electron diffraction study of this phase[28] indicated a monoclinic cell of $P2/m$ symmetry that was modeled with lithium ions occupying half of the available octahedral sites between the CoO_2 layers in an ordered fashion. In our powder neutron diffraction patterns of $Li_{0.51}CoO_2$, however, the extra reflections that would result from the presence of ordered lithium ions were not observed. This suggests that if present the Li ordering is only over short ranges and can only be observed by electron diffraction. The refinements were therefore carried out in the $C2/m$ space group (12), in which the Li fills half the available octahedral sites between the CoO_2 layers in a disordered fashion. The relationship between the rhombohedral and monoclinic structures for Li_xCoO_2 is shown in Fig. 9.

The structural characteristics of the Li-O plane in Li_xCoO_2 are presented in Fig. 10. The upper panel shows the composition dependent variation of the Li-O layer thickness, determined by calculating the perpendicular distance be-

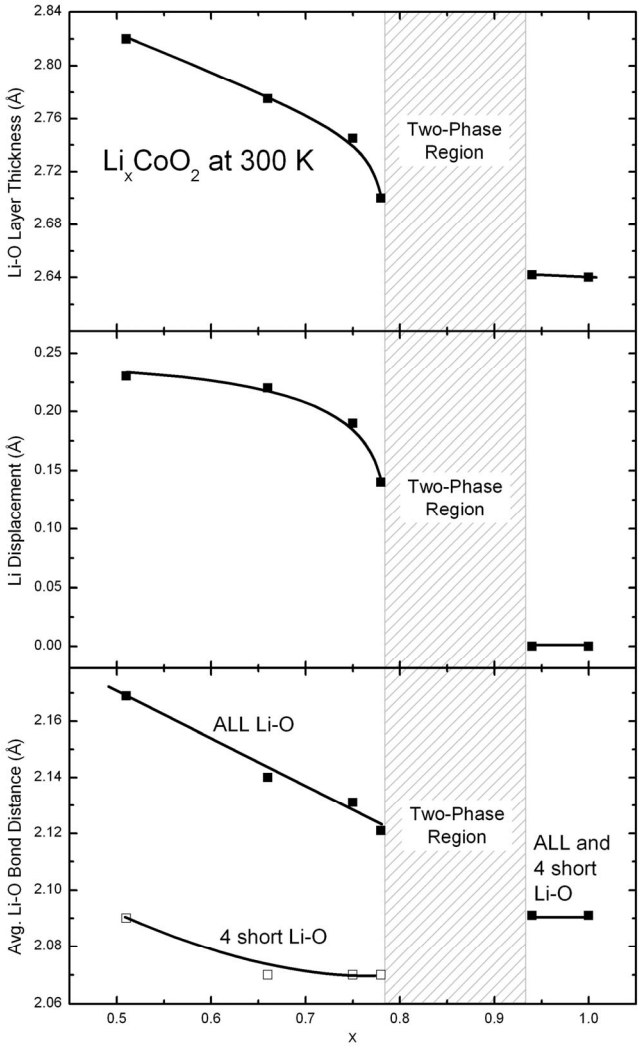

FIG. 10. The Li-O plane characteristics in Li_xCoO_2. Upper panel: Variation of the Li layer thickness with x. Middle panel: The magnitude of the displacement of the lithium ions from their ideal octahedral sites. Lower panel: The average Li-O bond distance taken over all oxygen, and the average taken over four nearest oxygen.

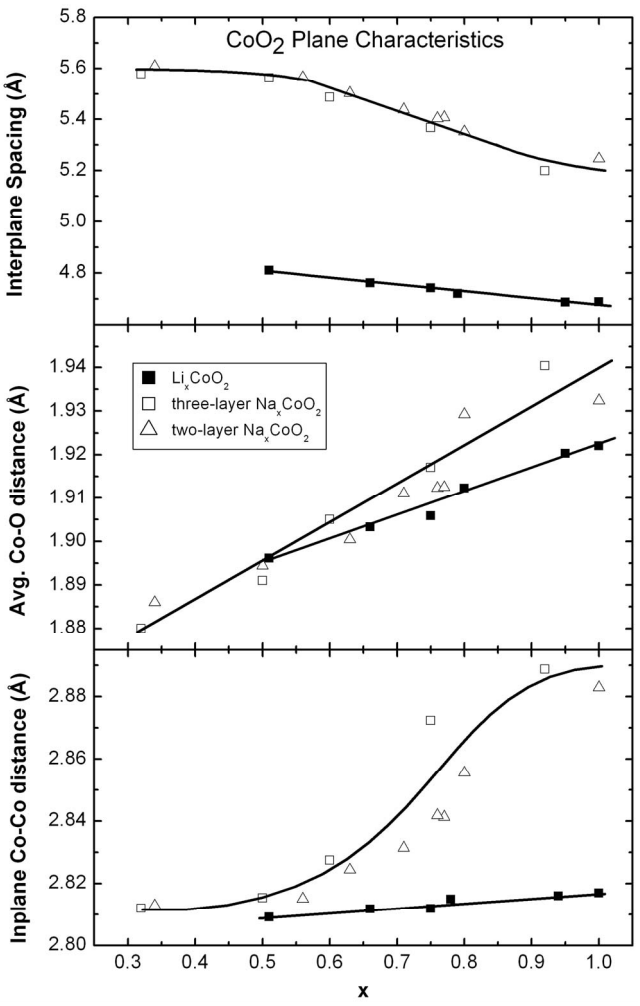

FIG. 11. Comparison of the CoO_2 plane characteristics in Li_xCoO_2 and Na_xCoO_2 (Refs. 4 and 10). Upper panel: The distance between CoO_2 layers as a function of Li (Na) content. Middle panel: The variation of average Co-O bond length with Li(Na) content. Lower panel: The variation in in-plane Co-Co distance as a function of Li (Na) content.

tween adjacent planes of oxygen anions separated by Li. As is seen in other systems, the removal of the strongly bonding alkali ions from between the CoO_2 layers causes the layers to move further apart as their repulsion overcomes the bonding forces holding them together. The LiO_6 coordination polyhedra, which are already large in $LiCoO_2$ (Li-O bond length 2.09 Å), further increase in size as the layers move apart. This increase of the interplane spacing drives the Li off-center within the oxygen coordination polyhedra so they can preserve favorable Li-O bonding distances. With a significant fraction of the Li sites vacant in the composition region $0.51 < x < 0.78$, this is possible because in-plane repulsion of neighboring Li is relaxed. The middle panel of Fig. 10 plots the magnitude of the displacement of the lithium ions from their ideal octahedral sites versus lithium content; they become increasingly displaced as the Li-O layer expands. As the lower panel of Fig. 10 shows, the average Li-O bond distance increases substantially as lithium is removed. That is, the LiO_6 octahedra become stretched significantly in the c direction as x decreases, resulting in longer average Li-O bonds. However, the displacements are such that the Li stays close to four of its six neighboring oxygens in spite of the expansion of the oxygen polyhedron, maximizing the bonding interactions with those four oxygen at the expense of the interactions with the other two. Although the average Li-O bond distance increases substantially as x decreases, the average distance from the Li to the four nearest oxygen remains relatively constant throughout the series, seen in the lower panel to Fig. 10. Thus, once the lithium layer has been partially depopulated, the lithium ions displace from their ideal octahedral sites to maintain strong bonding interactions with some of their oxygen neighbors.

Neutron diffraction studies of the two- and three-layer Na_xCoO_2 systems have quantified changes in Co-O bond length, in-plane Co-Co distance, and the interplane spacing. The variations of these characteristics for Li_xCoO_2 are compared with those in two- and three-layer Na_xCoO_2 in Fig. 11;

TABLE V. Summary of significant structural parameters in Li_xCoO_2.

Lithium content (x)	Li layer thickness (Å)	Avg. Li-O distance (Å)	Li displacement (Å)	Avg. four shortest Li-O Bonds (Å)	Observed CoO_2 layer thickness T_{obs} (Å)	Ideal CoO_2 layer thickness T_{ideal} (Å)	T_{obs}/T_{ideal}
1.00	2.640	2.09	0	2.09	2.048	2.300	0.890
0.94	2.641	2.09	0	2.09	2.046	2.299	0.890
0.78	2.700	2.12	0.14(3)	2.07	2.020	2.298	0.879
0.75	2.745	2.13	0.19(1)	2.07	1.997	2.296	0.870
0.66	2.775	2.14	0.22(1)	2.07	1.987	2.296	0.865
0.51	2.819	2.17	0.23(1)	2.09	1.965	2.294	0.857

they change much more dramatically in Na_xCoO_2 than in Li_xCoO_2. On increasing x from 0.5 to 1.0, the Co-O bond distance increases by 0.45 Å for Na_xCoO_2, but only by 0.26 Å for Li_xCoO_2. Similarly, the Co-Co distance within the CoO_2 plane, reflecting the in-plane size of the CoO_6 octahedra, increases by 0.74 Å for Na_xCoO_2, but only by 0.08 Å for Li_xCoO_2—a nearly tenfold difference. Finally, the spacing between CoO_2 planes decreases by 3.7 Å for Na_xCoO_2 but by half that, 1.8 Å, for Li_xCoO_2.

Near $x=0.5$, the Co-O bond lengths and in-plane Co-Co distances are quite similar in the sodium and lithium systems (Fig. 11). As described above, these two structural parameters increase substantially with increasing x in Na_xCoO_2, while only changing slightly in Li_xCoO_2. Most dramatically, the CoO_2 layer expands considerably in the in-plane dimension in the sodium system, but not in the lithium system. It may be that the relatively large size of the sodium ions [radius=1.04 Å (Ref. 59)] causes crowding that gives rise to the dramatic expansion of the CoO_2 layer in Na_xCoO_2: As the sodium layer becomes filled, the CoO_2 layer must stretch in plane to accommodate the coordination of bulky sodium ions to the oxygen anions. Alternatively, it could be that rather than the sodium ions being too large, the lithium ions are too small: The more compact lithium ions [radius =0.74 Å (Ref. 59)] may restrict what the electronic energies would prefer, the in-plane expansion of the CoO_2 layer, because this expansion would overstretch the Li-O bonds. Whatever the underlying cause, the geometries of the CoO_2 layers are very different for $0.5<x<1.0$ in Li_xCoO_2 and Na_xCoO_2.

DISCUSSION

The structural characteristics of the CoO_2 layers in Na_xCoO_2 and Li_xCoO_2 directly impact their electronic systems. The in-plane expansion of the CoO_2 layer observed when $x>0.75$ in Na_xCoO_2 (Fig. 11) suggests that gradual but significant changes in electronic band occupancy occur at that composition, whereas the much smaller change in size of the CoO_2 plane in Li_xCoO_2 suggests that the electronic system does not undergo qualitative changes in that case. We have previously proposed that the distortion of the CoO_6 octahedron is an important indicator of the electronic state of Na_xCoO_2,[10] due to the expectation that the shape of the CoO_6 octahedra will impact the energies of Co t_{2g} and e_g orbitals. To quantify this distortion, the in-plane Co-Co distance can be used to calculate the CoO_2 layer thickness that would be expected if the CoO_6 octahedra were ideal in shape—a situation that would lead to degeneracy among the three t_{2g} orbitals. This ideal layer thickness is then compared to the actual observed thickness of the CoO_2 layer to quantify how much the t_{2g} degeneracies might be lifted by the structural distortion. The relationship between the in-plane Co-Co distance ($d_{Co\text{-}Co}$) and the thickness of a layer of ideal edge-sharing CoO_6 octahedra (T_{ideal}) is $T_{ideal}=(\sqrt{6}/3)\,d_{Co\text{-}Co}$. By determining the ratio of the observed layer thickness to the ideal layer thickness T_{obs}/T_{ideal}, as enumerated in Table V, the degree of the distortion of the CoO_6 octahedra can be obtained. If this ratio is less than 1, as it is in these systems, then the CoO_6 octahedra are compressed perpendicular to the CoO_2 planes.

Comparison of the variation of T_{obs}/T_{ideal} with alkali content for three-layer Li_xCoO_2, two-layer Na_xCoO_2, and three-layer Na_xCoO_2 is shown in Fig. 12. As lithium content decreases in Li_xCoO_2, the CoO_2 octahedra are monotonically

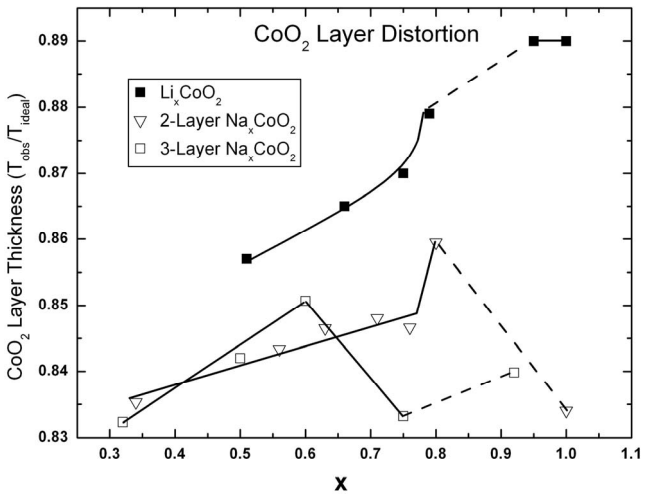

FIG. 12. The variation of the T_{obs}/T_{ideal} ratio with x for Li_xCoO_2 and two- and three-layer Na_xCoO_2 (Refs. 4 and 10).

more compressed perpendicular to the plane. The behavior in the Na_xCoO_2 systems is much more complex, suggesting significant electronic reconfigurations across the series. Further, at least in the range $0.5 \leqslant x \leqslant 1.0$, the CoO_6 octahedra are significantly more distorted in Na_xCoO_2 than in Li_xCoO_2, suggesting that the electronic systems are quite different in these families.

CONCLUSIONS

Our study of the magnetic properties and structural characteristics of Li_xCoO_2 leads us to infer that the structural rigidity of this family is a critical factor in determining why it displays much more conventional magnetic properties than are seen in Na_xCoO_2. Unexpected, however, is that analysis of the magnetic data shows that the spin state of Co^{4+} in Li_xCoO_2 changes from high spin at compositions above the two-phase region to low spin at compositions below the two-phase region. It is unclear why this high-spin to low-spin transition is not observed in the high x region of Na_xCoO_2, since the larger Co-O octahedra observed there would be expected to be more favorable to the existence of high-spin Co^{4+}, but it may be that further detailed study is needed on this issue.[60,61] In all $Alkali_xCoO_2$ systems studied thus far, a chemical two-phase region is observed for $x \approx 0.8-0.9$. Whether this phase separation is chemically or electronically driven is not currently understood, but total energy calculations have been interpreted as saying that it cannot be driven by Li/vacancy ordering.[62] Finally, though this study has established correlations between the structures and properties of Na_xCoO_2 and Li_xCoO_2, it has not elucidated the basic physics that underlies those correlations. Because the triangular CoO_2 planes found in these cobaltates differ substantially in phenomenology from the square planes commonly studied in perovskites, further theoretical and experimental study of their structure-property relations would clearly be of future interest.

ACKNOWLEDGMENTS

The research at Princeton University is supported by the U.S. Department of Energy, Division of Basic Energy Sciences, Grant No. DOE-FG98-02-45706.

[1] I. Terasaki, Y. Sasago, and K. Uchinokura, Phys. Rev. B **56**, R12685 (1997).
[2] K. Takada, H. Sakurai, E. Takayama-Muromachi, F. Izumi, R. A. Dilanian, and S. Sasaki, Nature (London) **422**, 53 (2003).
[3] M. L. Foo, Y. Wang, S. Watauchi, H. W. Zandbergen, T. He, R. J. Cava, and N. P. Ong, Phys. Rev. Lett. **92**, 247001 (2004).
[4] Q. Huang, M. L. Foo, R. A. Pascal, Jr., J. W. Lynn, B. H. Toby, T. He, H. W. Zandbergen, and R. J. Cava, Phys. Rev. B **70**, 184110 (2004).
[5] J. D. Jorgensen, M. Avdeev, D. G. Hinks, J. C. Burley, and S. Short, Phys. Rev. B **68**, 214517 (2003).
[6] R. Jin, B. C. Sales, S. Li, and D. Mandrus, Phys. Rev. B **72**, 060512(R) (2005).
[7] Y. Takahashi, Y. Gotoh, and J. Akimoto, J. Solid State Chem. **172**, 22 (2003).
[8] Y. Ono, R. Ishikawa, Y. Miyazaki, Y. Ishii, Y. Morii, and T. Kajitani, J. Solid State Chem. **166**, 177 (2002).
[9] C. Fouassier, G. Matejka, J.-M. Reau, and P. Hagenmuller, J. Solid State Chem. **6**, 532 (1973).
[10] L. Viciu, J. W. G. Bos, H. W. Zandbergen, Q. Huang, M. L. Foo, S. Ishiwata, A. P. Ramirez, M. Lee, N. P. Ong, and R. J. Cava, Phys. Rev. B **73**, 174104 (2006).
[11] H. F. Gibbard, J. Power Sources **26**, 81 (1989).
[12] K. Mizushima, P. C. Jones, P. J. Wiseman, and J. B. Goodenough, Mater. Res. Bull. **15**, 783 (1980).
[13] T. Ohzuku, A. Ueda, M. Nagayama, Y. Iwakoshi, and H. Komori, Electrochim. Acta **38**, 1159 (1993).
[14] C. Delmas, J. J. Braconnier, and P. Hagenmuller, Mater. Res. Bull. **17**, 117 (1982).
[15] D. Carlier, I. Saddoune, M. Menetrier, and C. Delmas, J. Electrochem. Soc. **149**, A1310 (2002).
[16] D. Carlier, I. Saddoune, L. C. Roguennec, M. Menetrier, E. Soard, and C. Delmas, Solid State Ionics **144**, 263 (2001).
[17] R. J. Gummow, M. M. Thackary, W. I. F. David, and S. Hull, Mater. Res. Bull. **27**, 327 (1992).
[18] E. Rossen, J. N. Reimers, and J. R. Dahn, Solid State Ionics **62**, 53 (1993).
[19] R. Gupta and A. Manthiram, J. Solid State Chem. **121**, 483 (1996).
[20] V. R. Galakhov, N. A. Ovechkina, A. S. Shkvarin, S. N. Shamin, E. Z. Kurmaev, K. Kuepper, A. F. Takács, M. Raekers, S. Robin, M. Neumann, G.-N. Gavrilă, A. S. Semenova, D. G. Kellerman, T. Käämbre, and J. Nordgen, Phys. Rev. B **74**, 045120 (2006).
[21] N. Imanishi, M. Fujiyoshi, Y. Takeda, O. Yamamoto, and M. Tabuchi, Solid State Ionics **118**, 121 (1999).
[22] L. A. Montoro, M. Abbate, and J. M. Rosolen, Electrochem. Solid-State Lett. **3**, 410 (2000).
[23] S. Venkatraman and A. Manthiram, Chem. Mater. **14**, 3907 (2002).
[24] S. Levasseur, M. Menetrier, E. Suard, and C. Delmas, Solid State Ionics **128**, 11 (2000).
[25] G. G. Amatucci, J. M. Tarascon, and L. C. Klein, J. Electrochem. Soc. **143**, 1114 (1996).
[26] J. N. Reimers and J. R. Dahn, J. Electrochem. Soc. **139**, 2091 (1992).
[27] J. S. Hong and J. R. Selman, J. Electrochem. Soc. **147**, 3183 (2000).
[28] Y. Shao-Horn, S. Levasseur, F. Weill, and C. Delmas, J. Electrochem. Soc. **150**, A366 (2003).
[29] M. Menetrier, I. Saddoune, S. Levasseur, and C. Delmas, J. Mater. Chem. **9**, 1135 (1999).
[30] H. J. Orman and P. J. Wiseman, Acta Crystallogr., Sect. C: Cryst. Struct. Commun. **40**, 12 (1984).
[31] T. A. Hewston and B. L. Chamberland, J. Phys. Chem. Solids **48**, 97 (1987).
[32] Y. Takahashi, N. Kijima, K. Dokko, M. Nishizawa, I. Uchida, and

J. Akimoto, J. Solid State Chem. **180**, 313 (2007).
[33] J. Sugiyama, H. Nozaki, J. H. Brewer, E. J. Ansaldo, G. D. Morris, and C. Delmas, Physica B **374**, 148 (2006).
[34] J. Sugiyama, H. Nozaki, J. H. Brewer, E. J. Ansaldo, G. D. Morris, and C. Delmas, Phys. Rev. B **72**, 144424 (2005).
[35] D. G. Kellerman, V. R. Galakhov, A. S. Semenova, Ya. N. Blinovskov, and O. N. Leonidova, Phys. Solid State **48**, 548 (2006).
[36] D. G. Kellerman, V. V. Karelina, Ya. N. Blinovskov, and A. I. Gusev, Russ. J. Inorg. Chem. **47**, 884 (2002).
[37] S. Levasseur, M. Menetrier, Y. Shao-Horn, L. Gautlier, A. Audemer, G. Demazeau, A. Largeteau, and C. Delmas, Chem. Mater. **15**, 348 (2003).
[38] C. A. Marianetti, G. Kotliar, and G. Ceder, Nat. Mater. **3**, 627 (2004).
[39] M. H. Whangbo, D. Dai, and R. K. Kremer, Inorg. Chem. **45**, 5989 (2006).
[40] G. Lang, J. Bobroff, H. Alloul, P. Mendels, N. Blanchard, and G. Collin, Phys. Rev. B **72**, 094404 (2005).
[41] T. Yamamoto, K. Uchinokura, and I. Tsukada, Phys. Rev. B **65**, 184434 (2002).
[42] M. Hervieu, Ph. Boullay, C. Michel, A. Maignan, and B. Raveau, J. Solid State Chem. **142**, 305 (1999).
[43] D. Pelloquin, S. Hebert, A. Maignan, and B. Raveau, J. Solid State Chem. **178**, 769 (2005).
[44] I. Terasaki, Physica B **328**, 63 (2003).
[45] S. Choi and A. Manthiram, J. Solid State Chem. **164**, 332 (2002).
[46] E. Antolini, Solid State Ionics **170**, 159 (2004).
[47] S. Kikkawa, S. Miyazaki, and M. Koizumi, J. Solid State Chem. **62**, 35 (1986).
[48] A. Lundblad and B. Bergman, Solid State Ionics **96**, 173 (1997).
[49] A curve was fitted to our data relating amount of Br_2 employed and final Li content, determined by ICP-AES, in Li_xCoO_2. This curve had the form $\hat{x}=0.441+0.846/(R+1.454)$, where R is the molar ratio of Br_2 to $LiCoO_2$, and $\hat{x}$ is the lithium content of the deintercalated compound. This equation was used to estimate the amount of Br_2 needed to achieve a target Li stoichiometry in deintercalated products.
[50] Previous studies have demonstrated a monotonic relationship between unit cell parameters and lithium content in Li_xCoO_2 (Refs. 21, 24–27, and 32). To establish Li concentrations to sufficient precision for comparing the different types of samples used in this study, quantitative calibration curves were established relating unit cell parameters to composition by refining the unit cell parameters by powder x-ray diffraction and measuring the ICP-AES compositions of 17 calibration samples. Separate linear regressions were performed on either side of the two-phase region. For $0.5 \leqslant x \leqslant 0.78$, the regression yielded $x=21.857-(1.480\ \text{Å}^{-1})\times c$, where x is the lithium content and c is the c-axis parameter (in Å), with a standard error in x of 0.014. For $0.94 \leqslant x \leqslant 1.00$, the regression yielded $x=23.241-(1.581\ \text{Å}^{-1})\times c$, with a standard error of 0.015 for x. These equations were used in all investigations to determine precise compositions of various Li_xCoO_2 samples from their refined c-axis parameters.
[51] H. Kawaji, M. Takematsu, T. Tojo, T. Atake, A. Hirano, and R. Kanno, J. Therm Anal. Calorim. **68**, 833 (2002).
[52] M. Carewska, A. DiBartolomeo, and S. Scaccia, Thermochim. Acta **269**, 491 (1995).
[53] A. Larson and R. B. Von Dreele, GSAS, Generalized Structure Analysis System, Los Alamos National Laboratory, Los Alamos, NM, 1994.
[54] N. W. Ashcroft and N. D. Mermin, *Solid State Physic* (Harcourt College, Fort Worth, 1976).
[55] W. B. Wu, D. J. Huang, J. Okamoto, A. Tanaka, H.-J. Lin, F. C. Chou, A. Fujimori, and C. T. Chen, Phys. Rev. Lett. **94**, 146402 (2005).
[56] T. Kroll, M. Knupfer, J. Geck, C. Hess, T. Schwieger, G. Krabbes, C. Sekar, D. R. Batchelor, H. Berger, and B. Büchner, Phys. Rev. B **74**, 115123 (2006).
[57] T. Kroll, A. A. Aligia, and G. A. Sawatzky, Phys. Rev. B **74**, 115124 (2006).
[58] G. A. Sawatzky (private communication).
[59] R. D. Shannon and C. T. Prewitt, Acta Crystallogr., Sect. B: Struct. Crystallogr. Cryst. Chem. **25**, 925 (1969).
[60] C. Bernhard, Ch. Neidermayer, A. Drew, G. Khaliullin, S. Bayracki, J. Strempfer, R. K. Kremer, D. P. Chen, C. T. Lin, and B. Keimer, Europhys. Lett. **80**, 27005 (2007).
[61] C. de Vaulx, M.-H. Julien, C. Berthier, M. Horvatić, P. Bordet, V. Simonet, D. P. Chen, and C. T. Lin, Phys. Rev. Lett. **95**, 186405 (2005).
[62] A. Van der Ven, M. K. Aydinol, G. Ceder, G. Kresse, and J. Hafner, Phys. Rev. B **58**, 2975 (1998).